Refractive index and gain grating in Nd:YVO4: application to speckle vibrometry and photoacoustic detection

Baptiste Jayet, Jean-Pierre Huignard, Francois Ramaz

Refractive index and gain grating in Nd:YVO_4: Application to speckle vibrometry and photoacoustic detection.

Baptiste Jayet[1,†], Jean-Pierre Huignard[2], and Francois Ramaz[1,*]

[1] *Institut Langevin, ESPCI Paris, PSL Research University, CNRS UMR7587, INSERM U979, UPMC, 1 rue Jussieu, 75005 Paris, France*
[2] *Jphopto-consultant, 20 rue Campo Formio, 75013 Paris, France*
[†] *Current address: Optics and Photonics, The University of Nottingham, NG72RD, Nottingham, United Kingdom*
[*] *Corresponding author: francois.ramaz@espci.fr*

Compiled January 5, 2017

Probing local displacements on a scattering surface can be achieved using an adaptive interferometer. Photorefractive-crystal based interferometer are popular, but alternatives exist, such as Adaptive Gain interferometer. Such setups take advantage of the non linear phenomena in laser media. Because of the gain saturation, it is possible to write a gain hologram and a refractive index hologram to achieve an adaptive interferometer with a linear response. In addition, laser media based setups have a fast response time (≤ 100 µs), which makes them interesting for application such as detection of photoacoustic waves in living biological samples.

OCIS codes: *(090.2880), (110.0113), (110.7170), (110.5120), (140.4480), (170.3880)*

Remote sensing of vibrations is currently commonly used in industry for non-destructive testing (NDT). Indeed, using an interferometer to probe the displacement of the surface of an object gives information on how acoustic wave propagate inside, which, in turn, gives information about the internal structure of the object. Hochreiner *et. al.* showed that it was possible to use the same methods used in NDT for the detection of photoacoustic signals during photoacoustic imaging on living organisms [1]. One of the main advantage of this optical measurement is its contactless nature, which is interesting when working on sensitive samples, *i. e.*, that needs to be isolated from pollution.

When performing interferometry on an optically scattering surface, such as biological media, the use of a classic interferometry setup results in a poor sensitivity, typically limited to the signal to noise ratio (SNR) of one speckle grain. One solution to compensate for the low spatial correlation of the wavefront backscattered by the moving sample, is to add a dynamic wavefront adaption stage into the interferometer. This is usually done using holographic two-wave mixing in photorefractive crystals [2]. This process consists in generating a complex reference wavefront with the same spatial modulation (speckle) instead of a plane wave. This will result in a spatial matching of both wavefronts and therefore a coherent summation of the vibrating signal of each speckle grains on a large surface single detector and an increased SNR [3]. In the right configuration, a sensitive linear response – with respect to phase changes – of the interferometer can be achieved. This photorefractive adaptive holography setup has revealed to be efficient and is currently used in commercial products for industrial NDT applications.

Another way of performing wave-mixing and wavefront adaption consist in exploiting gain saturation in laser media [4, 5]. Such media offer the possibility to perform dynamic holography with a sub-millisecond response time – typically between 100 µs and 200 µs – which is of great interest for applications such as optical metrology [6] or acousto-optic detection for tissue imaging [7]. Adaptive gain interferometers (AGI), due to their local spatial response (gain grating in phase with illumination fringes) have a quadratic response, *i. e.*, the modulated component of the light intensity at the output of the interferometer is proportional to the square of magnitude of the phase modulation [7]. Thus making the signal very weak in case of a small phase modulation. However, in certain conditions, the spatial modulation of the gain may induce a spatial modulation of the refractive index of the material [8]. For example, a wavelength mismatch between the amplified light and the wavelength corresponding to the maximum of the gain characteristic of the amplifier, can cause a phase shift, which corresponds to a phase grating. Usually, this additional phase grating is neglected, but recent works suggest that it can be efficiently exploited [9, 10]. As this refractive index grating is local, it directly yields a linear response of the interferometer resulting in a much higher sensi-

tivity than the quadratic response given by the gain grating.

In this letter, we report an experimental observation of both contributions – gain grating and refractive index grating – in an AGI based on a Nd:YVO_4 laser crystal with a probe beam generated by a Nd:YAG laser and show the promising results of the detection of photoacoustic waves on a phantom mimicking a biological media. First the observations are compared to

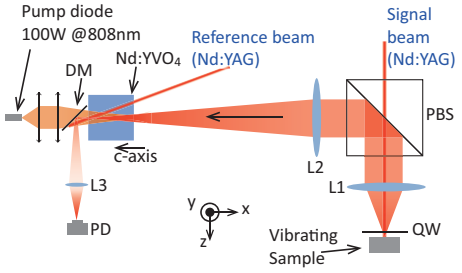

Fig. 1. Nd:YVO_4-based AGI. PBS, polarising beamsplitter; QW, quarter-wave plate; L*i*, *i*-th lens; DM, dichroic mirror; PD, photodiode

a theoretical model adapted from the wave-mixing model presented in [7]. Secondly, we report an original application of our interferometer: the non contact detection of photoacoustic signals for imaging biological tissues. Our AGI (see Fig. 1) is composed of a *c*-cut, $5 \times 5 \times 5\,\mathrm{mm}^3$ Nd:YVO_4 crystal (Crylight Photonics Inc.). The front side – where the reference and signal beams enter the crystal – is antireflection (AR) coated for 1064 nm, whereas the back side – where the pump enters – is AR coated both for 1064 nm and 808 nm (Pumping wavelength). The crystal is pumped by a high power 808 nm pump diode capable of providing up to a 100 W-CW (LIMO100-F200-DL808). In order to avoid thermal damage, the crystal is water-cooled at around 20 °C and pumped in a Quasi Continuous Wave (QCW) regime (1 ms-long pulse at a 10 Hz repetition rate). The light from the pump is focused in the crystal by a 18 mm-focal length lens in order to have a pumped volume of about $0.4\,\mathrm{mm}^3$. The probe beam is generated by a CW-1W single longitudinal mode Nd:YAG (CrystaLaser inc.), coupled to a 5W Yb-doped fiber amplifier (Keopsys inc.) and split into two beams (reference and signal) by a combination of half-wave plate and polarizing beamsplitter (not represented in Fig. 1). After travelling through the crystal, the 1064 nm light is separated from the pump by a dichroic mirror.

As described in [11], there are two contributions to the additional refractive index grating: a non-resonant one (due to the UV absorption bands) and a resonant one (due to an eventual wavelength mismatch between the probe light and maximum of the material's laser transition). The model of two-wave mixing in a gain medium developed in [7] can be adapted to take into account the refractive index modulation. This yields the following equation for the optical field at the output of the gain crystal:

$$E_S(z,t) = G(E_S(0,t) + E_S(0,t) * C(z,t) + i\beta E_S(0,t) * C(z,t)) \quad \textbf{(1)}$$

Where G is the gain factor within the crystal, $E_S(0,t)$ is the transmitted signal beam, $E_S(0,t) * C(z,t)$ is the diffracted reference on the gain hologram and $i\beta E_S(0,t) * C(z,t)$ is the diffracted reference on the refractive index hologram. In this last term appears the Henry like Factor β, which quantifies the contribution of the refractive index grating. It can be decomposed into the sum of two terms: $\beta = \beta_{NR} + \beta_R$, respectively linked to the non-resonant and to the resonant contributions [10]. Considering our experimental conditions, *i. e.* diode pumping and wavelength difference between Nd:YAG and Nd:YVO_4, we used the expressions given by R. Soulard in [10] to evaluate β_{NR} and β_R respectively at 0.08 and 0.22. Hence, with our experimental conditions, the refractive index grating is mainly due to the wavelength mismatch between the Nd:YAG probe laser ($\lambda_0 =$ 1064.2 nm) and the Nd:YVO_4 amplifier ($\lambda_{em} = 1064.3$ nm).

In order to observe the response of our AGI to a phase-modulated speckle light, we use a piece of white paper glued on a silicon wafer itself mounted on a piezoelectric ceramic. This "sample" is placed as indicated in Fig. 1 (vibrating sample). The backscattered light is modulated by the vibrating piezoelectric ceramic, which is supplied by a sinusoidal voltage at $f_p = 40$ kHz. The signal from the photodiode is then high-pass filtered (butterworth filter at 5 kHz) before being digitized by a DAQ device (ADLINK PCI9646D). Time signals are recorded for several values of the displacement magnitude, which are changed by setting the voltage applied to the ceramic. An example of the Fourier spectrum of the acquired signal is reported in Fig. 2. As shown by Fourier spectrum, the response of our

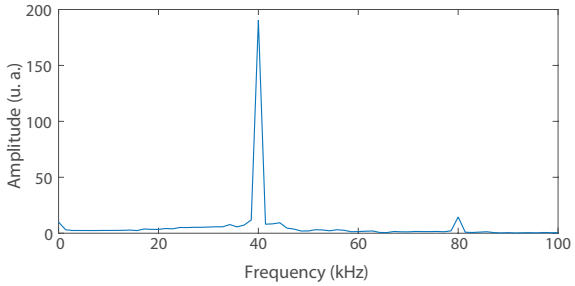

Fig. 2. Fourier spectrum of the signal acquired by the AGI while the paper is vibrating at $f_p = 40$ kHz.

setup to a sinusoidally phase-modulated speckle light has two contributions: a linear one – at f_p – and a quadratic one – at $2f_p$. The component at $2f_p$ was expected since the diffraction on a gain grating yields a quadratic response. The additional linear component, at f_p, is a proof of the presence of a local refractive index grating inside the crystal.

In order to characterise the response of our AGI, we can plot the magnitude of the peaks at f_p and $2f_p$ versus the displacement of the piezoelectric ceramic, *i. e.* versus the maximum voltage applied to the ceramic. Figure 3 shows the variations of each component versus the amplitude of the phase modulation, which is given by:

$$\Phi_0 = 2\frac{2\pi\mu V}{\lambda} \quad \textbf{(2)}$$

where μ is the piezoelectric coefficient of the ceramic (in $\mathrm{nm\,V^{-1}}$) and V is the voltage. The experimental data are acquired with an averaging over 100 acquisitions in order to estimate the standard deviation which is represented by the errorbars. The data are fitted using a theoretical model adapted from the model exposed in [7]. In the new model (more detail in chapter 7 of [12]), the variation of the refractive index has been taken into account by adding an imaginary part to the gain α. As predicted by the model, the two contributions – at f_p and $2f_p$ – can be observed. Moreover, taking into account our experimental conditions, our model can be adjusted in order to fit the

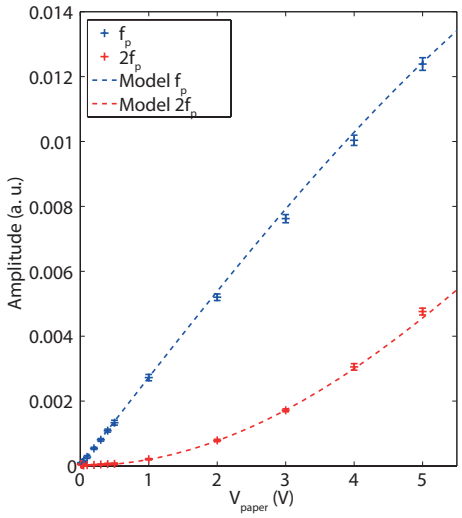

Fig. 3. Amplitude of the linear (blue) and quadratic (red) components. The dots represent the experimental data and the dashed line is the model.

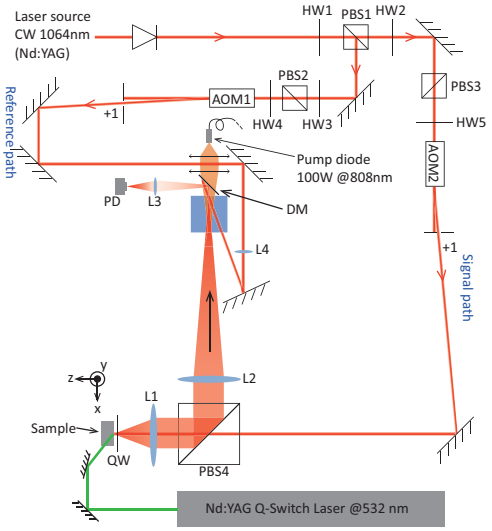

Fig. 4. Setup for the detection of photoacoustic signals. HW*i*, half-wave plate; PBS*i*, polarising beamsplitter; AOM*i*, acousto-optic modulators; L*i*, lens; QW quarter-wave plate; DM, dichroic mirror.

experimental data well. This first experiment confirms the presence of two gratings during the two wave-mixing process in our setup. As expected, the linear component – due to the refractive index grating – is much more sensitive than the quadratic one, especially at low displacement (in this experiment, the order of magnitude of the lowest displacement is around a few Å).

As proposed by Hochreiner *et. al*, it is possible to use a wavefront adaptive interferometer to probe vibrations generated by a photoacoustic effect. In their experiment [1], they used a photorefractive crystal of BSO in order to probe the local variation of displacement on the surface of a sample during a photoacoustic experiment. This all-optical photoacoustic experiment has potential advantages over a classic piezoeletric detection such as non contact and a much larger bandwidth. We adapted this idea using a gain medium which provides a faster response time, more suited for *in vivo* experiments. The setup presented in Fig. 4 can be used to achieve an optical detection of photoacoustic signals with an holographic detection with Nd:YVO_4. To begin with, our sample was a clear gel of agar with one side covered with a piece of cooked chicken breast to mimic a scattering biological medium. Behind the meat was placed either a thin red fishing line (diameter $\approx$ 170 µm) or a black sewing wire (diameter $\approx$ 500 µm). The photoacoustic effect was generated using a pulsed Q-Switch laser operating at 532 nm (Quantel Brilliant, max. 150 mJ per pulse, working at half power). The 4 ns pulse from the Q-Switch laser was send through the weakly scattering part of the gel in order to maximize the photoacoustic effect. The temporal signals measured for both targets are represented in Fig. 5a and 5b. As expected, the smaller target (fishing line) gives a signal containing higher frequency components than the larger sewing wire.

It is now possible to record the displacement at several positions of the probe beam on the surface of the samples. Each of them have been scanned in a direction perpendicular to the wire using a PI-micos step motor, with a travel pitch of 100 µm over a total course of 8 mm. On Fig 6 are reported the time signals at each position for the fishing line (6a) and the sewing wire (6b). We can clearly see the curved shape of the acoustic wavefront reaching the surface of the sample. The additional

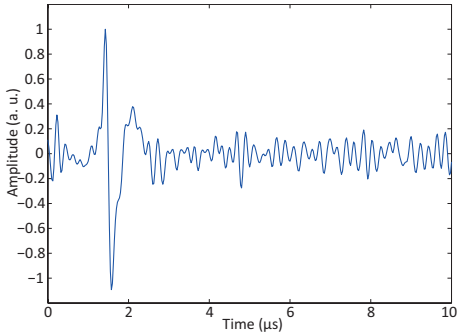

(a) Fishing line (170 µm)

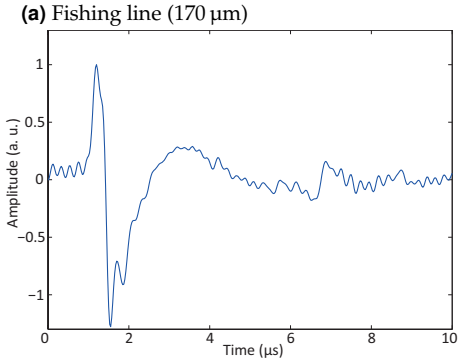

(b) Sewing wire (500 µm)

Fig. 5. Temporal photoacoustic signals for different targets

signals for $t \geq 5$ µs on the sewing wire data (Fig. 6b) can be attributed to a reflection of the ultrasonic wave on another edge of the surface (the wire was placed near a corner of the cubic sample). These data can be used as an input to reconstruct a photoacoustic image of the absorber. A beamforming algorithm developed for conventional photoacoustic imaging, *i. e.* with an array of transducer, was used to generate the images presented in Figs. 6c and 6d. The wires appears as dark spot on a gray background. Along the z-axis, the sizes of both wires fits

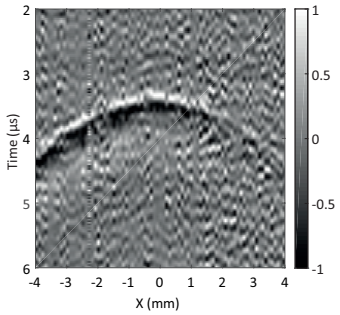

(a) Wavefront fishing line (170 µm)

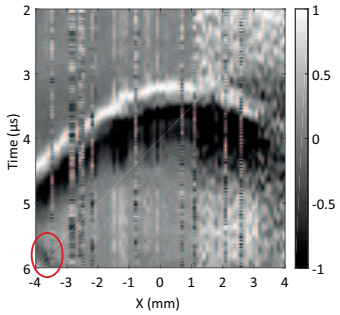

(b) Wavefront sewing wire (500 µm)

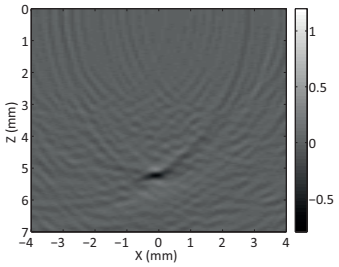

(c) Image fishing line (170 µm)

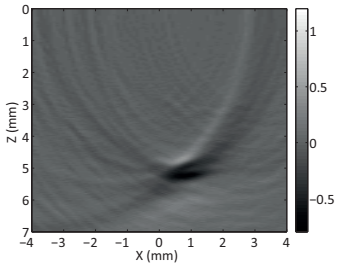

(d) Image sewing wire (500 µm)

Fig. 6. Time signals at different positions for the fishing line(a) and for the sewing wire(b) (The red circle corresponds to parasitic reflection on one of the edges of the gel.). Image after beamforming for the fishing line(c) and for the sewing wire(d).

the reality, whereas they seem stretched along the x-axis. This is due, on the one hand, by the limited collection angle of the acoustic wave (only 8 mm of the sample surface was scanned) and by the independent normalisation of each temporal signals. Indeed, because of the limited SNR, each recording has been pre-normalised to be able to exploit each line of the scan. As a result, the information on the relative amplitude of the wavefront has been lost, making the acoustic source appear larger than it really is.

As a conclusion, we have demonstrated the possibility of using an adaptive gain interferometer to remotely probe local displacements due to an acoustic wave generated through a photoacoustic effect. The originality of this AGI, which enables this detection, is the wavelength difference between the probe laser (generated by a Nd:YAG laser) and the crystal used for holography (Nd:YVO_4). This wavelength difference allows for the creation of an additional refractive index grating that has a non-negligible contribution, as shown by the value of the resonant contribution of the Henry factor. Currently, the sensitivity of this setup is not as good as what is achieved with piezoelectric probes. Also the acquisition is done point by point and not in parallel like with a multi-element probe. However the use of an AGI has great benefits. Firstly it provides a non-contact measurement which may be of interests in situation where the tested sample is not directly accessible or cannot be touched. Secondly, compared to photorefractive crystal based setup, the response time is much faster (< 100 µs vs. a few ms). This provides a good shield against low frequency noise. Namely, the setup will be able to compensate parasitic vibrations with a frequency of the order of magnitude of a few 10 kHz, while still be able to detect the *in vivo* photoacoustic signals that usually have frequencies in the MHz range. Finally, optical detections have a very large bandwidth compared to usual ultrasonic probes therefore is it possible to use the same setup to measure signal in various frequency range to access different scales of details.

FUNDING INFORMATION

Direction générale de l'Armement; *Agence Nationale de la Recherche* (ICLM-ANR-2011-BS04-017-01); *Fondation Pierre-Gilles De Gennes*; *LABEX WIFI* (ANR-10-IDEX-0001-02 PSL).

REFERENCES

1. A. Hochreiner, T. Berer, H. Grün, M. Leitner, and P. Burgholzer, Journal of Biophotonics **5**, 508 (2012).
2. A. A. Kamshilin, R. V. Romashko, and Y. N. Kulchin, Journal of Applied Physics **105**, 031101 (2009).
3. J.-P. Huignard and A. Marrakchi, Optics Letters **6**, 622 (1981).
4. M. J. Damzen, R. P. M. Green, and G. J. Crofts, Optics Letters **17**, 1331 (1992).
5. A. Brignon and J.-P. Huignard, Optics Letters **18**, 1639 (1993).
6. M. J. Damzen, A. Boyle, and A. Minassian, Optics Letters **30**, 2230 (2005).
7. B. Jayet, J.-P. Huignard, and F. Ramaz, Optics Express **22**, 20622 (2014).
8. O. L. Antipov, S. I. Belyaev, A. S. Kuzhelev, and D. V. Chausov, JOSA B **15**, 2276 (1998).
9. R. Soulard, A. Zinoviev, J. L. Doualan, E. Ivakin, O. Antipov, and R. Moncorge, Optics Express **18**, 1553 (2010).
10. R. Soulard, A. Brignon, J.-P. Huignard, and R. Moncorge, Journal of the Optical Society of America B **27**, 2203 (2010).
11. O. L. Antipov, A. S. Kuzhelev, A. Y. Luk'yanov, and A. P. Zinov'ev, Quantum Electronics **28**, 867 (1998).
12. B. Jayet, PhD Thesis, Université Pierre et Marie Curie - Paris VI (2015).

FULL REFERENCES

1. A. Hochreiner, T. Berer, H. Grün, M. Leitner, and P. Burgholzer, "Photoacoustic imaging using an adaptive interferometer with a photorefractive crystal," Journal of Biophotonics **5**, 508–517 (2012).
2. A. A. Kamshilin, R. V. Romashko, and Y. N. Kulchin, "Adaptive interferometry with photorefractive crystals," Journal of Applied Physics **105**, 031101 (2009).
3. J.-P. Huignard and A. Marrakchi, "Two-wave mixing and energy transfer in Bi12sio20 crystals: application to image amplification and vibration analysis," Optics Letters **6**, 622–624 (1981).
4. M. J. Damzen, R. P. M. Green, and G. J. Crofts, "High-reflectivity four-wave mixing by gain saturation of nanosecond and microsecond radiation in Nd:YAG," Optics Letters **17**, 1331–1333 (1992).
5. A. Brignon and J.-P. Huignard, "Two-wave mixing in Nd:YAG by gain saturation," Optics Letters **18**, 1639–1641 (1993).
6. M. J. Damzen, A. Boyle, and A. Minassian, "Adaptive gain interferometry: a new mechanism for optical metrology with speckle beams," Optics Letters **30**, 2230–2232 (2005).
7. B. Jayet, J.-P. Huignard, and F. Ramaz, "Fast wavefront adaptive holography in Nd:YVO4 for ultrasound optical tomography imaging," Optics Express **22**, 20622–20633 (2014).
8. O. L. Antipov, S. I. Belyaev, A. S. Kuzhelev, and D. V. Chausov, "Resonant two-wave mixing of optical beams by refractive-index and gain gratings in inverted Nd:YAG," JOSA B **15**, 2276–2282 (1998).
9. R. Soulard, A. Zinoviev, J. L. Doualan, E. Ivakin, O. Antipov, and R. Moncorge, "Detailed characterization of pump-induced refractive index changes observed in Nd:YVO_4, Nd:GdVO_4 and Nd:KGW," Optics Express **18**, 1553 (2010).
10. R. Soulard, A. Brignon, J.-P. Huignard, and R. Moncorge, "Non-degenerate near-resonant two-wave mixing in diode pumped Nd 3+ and Yb 3+ doped crystals in the presence of athermal refractive index grating," Journal of the Optical Society of America B **27**, 2203–2210 (2010).
11. O. L. Antipov, A. S. Kuzhelev, A. Y. Luk'yanov, and A. P. Zinov'ev, "Changes in the refractive index of an Nd:YAG laser crystal on excitation of the Nd3+ ions," Quantum Electronics **28**, 867 (1998).
12. B. Jayet, "Acousto-optic and photoacoustic imaging of scattering media using wavefront adaptive holography techniques in NdYO4," PhD Thesis, Université Pierre et Marie Curie - Paris VI (2015).